SCIENCE CHINA
Earth Sciences

• RESEARCH PAPER •

August 2013 Vol.56 No.8: 1434–1446
doi: 10.1007/s11430-012-4430-3

The projected temporal evolution in the interannual variability of East Asian summer rainfall by CMIP3 coupled models

FU YuanHai*

Climate Change Research Center, Chinese Academy of Sciences, Beijing 100029, China

Received January 6, 2012; accepted March 20, 2012; published online July 2, 2012

The projected temporal evolution in the interannual variability of East Asian summer rainfall in the 21st century is investigated here, by analyzing the simulated results of 18 coupled models under the 20th century climate experiment and scenario A1B. The multi-model ensemble (MME) mean projects two prominent changes in the interannual variability of East Asian summer rainfall in the 21st century under scenario A1B. The first change occurs around the 2030s, with a small change before and a large increase afterward. The intensity of the interannual variability increases up to approximately 0.53 mm/d in the 2070s, representing an increase of approximately 30% relative to the early 21st century. The second change happens around the 2070s, with a decrease afterward. By the end of the 21st century, the increase is approximately 12% relative to the early 21st century. The interannual variability of two circulation factors, the western North Pacific subtropical high (WNPSH) and the East Asian upper-tropospheric jet (EAJ), are also projected to exhibit two prominent changes around the 2030s and 2070 under scenario A1B, with consistent increases and decreases afterward, respectively. The MME result also projects two prominent changes in the interannual variability of water vapor transported to East Asia at 850 hPa, which occurs separately around the 2040s and 2070s, with a persistent increase and decrease afterward. Meanwhile, the precipitable water interannual variability over East Asia and the western North Pacific is projected to exhibit two prominent enhancements around the 2030s and 2060s and an increase from 0.1 kg/m^2 in the early 21st century to 0.5 kg/m^2 at the end of the 21st century, implying a continuous intensification in the interannual variability of the potential precipitation. Otherwise, the intensities of the three factors' (except EAJ) interannual variability are all projected to be stronger at the end of the 21st century than that in the early period. These studies indicate that the change of interannual variability of the East Asian summer rainfall is caused by the variability of both the dynamic and thermodynamic variables under scenario A1B. In the early and middle 21st century, both factors lead to an intensified interannual variability of rainfall, whereas the dynamic factors weaken the interannual variability, and the thermodynamic factor intensifies the interannual variability in the late period.

interannual variability, East Asian summer rainfall, future projection, climate change, climate model

Citation: Fu Y H. The projected temporal evolution in the interannual variability of East Asian summer rainfall by CMIP3 coupled models. Science China: Earth Sciences, 2013, 56: 1434–1446, doi: 10.1007/s11430-012-4430-3

Awareness of global warming and its influence on the Earth's environment is one of the most important advancements of meteorology in the 20th century. Climatic disasters and extreme climate events, such as droughts and floods, occur frequently in East Asia under global warming, resulting in enormous damages to society and economies. Therefore, making projections of future climate change in East Asia has been a key goal of climate change research.

The change of interannual variability is one of the important measurements of climate change and is closely related to the potential occurrence of droughts and floods. An intensified (weakened) change of interannual variability

*Corresponding author (email: fugreen1981@mail.iap.ac.cn)

indicates the increased (decreased) occurrence of climatic disasters. The East Asian summer precipitation exhibits a clear interannual variability, with the interannual standard deviation being approximately 6%–7% of the climatological mean [1]. Therefore, droughts and floods are the most serious disasters happening during the summer in East Asia, and they cause enormous damages.

Many studies have shown that summer precipitation increases in East Asia under global warming scenarios [2–10]. For example, Bueh [3] showed that the summer precipitation may significantly increase over the Yangtze (Changjiang) River valley and North China in the future. Sun and Ding [8] stated that summer precipitation may increase in East Asia and experience a prominent change around the 2040s with a large increase afterward. Li et al. [9] also suggested an intensified precipitation over most of China.

There are few studies on the possible change in the interannual variability of East Asian summer rainfall in the future. Recently, Kripalani et al. [1] showed that out of the 19 CMIP3 models, 13 depict significant increases in the interannual variability of the East Asian summer rainfall, but the multi-model ensemble (MME) mean showed no obvious change. By analyzing the simulation results of 12 CMIP3 models under scenarios A1B and A2, Lu and Fu [11] found that most of the selected models project an enhanced interannual variability of the East Asian summer rainfall in the 21st century, and the increased ratios of interannual variability of approximately 10% and 17% under scenarios A1B and A2, respectively, which are much stronger than those of the summer climatological precipitation.

Although the projected change in the interannual variability of East Asian summer rainfall in the future has been investigated, few studies have been performed on the temporal evolution of the interannual variability. We still have a paucity of knowledge for some important questions, such as whether the temporal evolution of the East Asian summer rainfall interannual variability experiences prominent change, how the change evolves in response to global warming, how the spatial pattern of precipitation variability changes, and what the roles of key dynamic and thermodynamic factors play in the process.

Unfortunately, numerical simulations for precipitation based on coupled models remain uncertain [12, 13], especially in East Asia, where there is a strong interaction between the lower and higher latitudes. Meanwhile, great uncertainties exist among models in simulating future climatological mean precipitation changes in East Asia [14, 15], and the MME results are even weaker than the dispersion among the models. For instance, Kitoh et al. [6] noticed a decreased precipitation in North China in summer, contrary to the results of Bueh [3] and Min et al. [4]. Therefore, we should also examine the changes in the interannual variability of dominant dynamic and thermodynamic components of the East Asian summer monsoon system, which are most closely related to the changes of East Asian summer precipitation interannual variability, to prove the changes of precipitation variability.

The interannual variation of East Asian summer precipitation is found to be closely related to local circulation anomalies as well as those in the western North Pacific [16]. The interannual variability of East Asian summer precipitation is closely related to anomalies of the western North Pacific subtropical high (WNPSH) in the lower troposphere and to the East Asian westerly jet (EAJ) in the upper troposphere. On the one hand, the WNPSH affects East Asian summer rainfall from south in the lower troposphere through zonal displacement. East Asia experiences flood (drought) when the WNPSH extends westward (retreats eastward) [17]. On the other hand, the EAJ affects East Asian summer rainfall from north in the upper troposphere through meridional displacement. A southward (northward) displaced EAJ favors above-normal (below-normal) precipitation in East Asia [18]. The relationships of East Asian summer rainfall with the WNPSH and EAJ remain robust in the 21st century [11].

Therefore, by analyzing the simulated results of 18 coupled models under the 20th century climate experiment (20C3M) and scenario A1B, we investigate the projected temporal evolution of the interannual variability of East Asian summer precipitation as well as the key dynamic components (the WNPSH, EAJ and water vapor transport) and thermodynamic component (precipitable water) of the East Asian summer monsoon system. In so doing, we attempt to obtain somewhat reliable projected changes of interannual rainfall variability in East Asia.

1 Models, data and methodology

We analyzed the results of 18 CMIP3 models for the 20C3M and scenario A1B. For both experiments, 100-year simulations (1901–2000 for 20C3M and 2001–2100 for A1B) are used to represent the 20th and 21st century climates. Table 1 lists the basic features of the selected models, and more detailed descriptions about the models can be found at http://www-pcmdi.llnl.gov/ipcc/about_ipcc.php.

The method of MME mean is used to analyze the projected change in interannual variability of the East Asian summer climate. The MME results are obtained by simply averaging over the available models with equivalent weight because uncertainty exists among the different models even under the same greenhouse gases and aerosol forcing and because there is no scientific way to evaluate the models. This method has been widely accepted and adopted in the climate change projection [8, 11, 19]. Many studies also suggest that the MME method has a better performance than individual models in reproducing the present climate in East Asia [13, 20–22].

Because the experiment number differs from model to

Table 1 Descriptions of the models used in this study

	Model I.D.	Abbreviation	Country	Resolution	Experiments	
					20C3M	A1B
01	BCCR-BCM2.0	bcm2.0	Norway	128×64, L17	1	1
02	CCSM3	ccsm3	USA	256×128, L17	7	7
03	CGCM3.1 (T47)	cgcm47	Canada	96×48, L17	5	5
04	CGCM3.1 (T63)	cgcm63	Canada	128×64, L17	1	1
05	CNRM-CM3	cnrm	France	128×64, L17	1	1
06	CSIRO-MK3.0	csiro3.0	Australia	192×96, L17	2	1
07	CSIRO-MK3.5	csiro3.5	Australia	192×96, L17	3	1
08	ECHAM5/MPI-OM	echam5	German	192×96, L16	4	4
09	FGOALS-G1.0	fgoals	China	128×60, L17	3	3
10	GFDL-CM2.0	gfdl2.0	USA	144×90, L17	3	1
11	GFDL-CM2.1	gfdl2.1	USA	144×90, L17	3	1
12	GISS-EH	giss	USA	72×46/45, L17	5	5
13	UKMO-HadCM3	hadcm3	UK	96×73/72, L15	2	1
14	UKMO-HadGEM1	hadgem	UK	192×145/144, L16	2	1
15	MIROC3.2 (hires)	miroch	Japan	320×160, L17	1	1
16	MIROC3.2 (medres)	mirocm	Japan	128×64, L17	3	3
17	MRI-CGCM2.3.2	mricgcm	Japan	128×64, L17	5	5
18	PCM	pcm	USA	128×64, L17	4	4

model (Table 1), the multi-experiment ensemble mean is obtained by averaging all the available simulations in the individual models with equivalent weight to each experiment. Then, all the data are converted to a spectral triangular wavenumber 42 truncation (T42, approximately 2.8×2.8 degrees latitude-longitude) resolution to enable MME analysis.

We use interannual standard deviations to depict the intensity of the interannual variability. A nine-year Gaussian filter is applied to the detrended data for the sake of eliminating the effect of decadal variability and to obtain the component of interannual variability.

To facilitate the quantitative investigation of precipitation and circulation, three indices are used in this study. Following Lu and Fu [11], we define the East Asian summer rainfall index (EASRI) as the June-July-August (JJA) mean precipitation averaged over the parallelogram region determined by the points (100°E, 25°N), (100°E, 35°N), (160°E, 30°N) and (160°E, 40°N), which is used to mimic the East Asian summer rain belt that is basically zonally-oriented but has a slight southwest-northeast tilt. This parallelogram region covers the region of the southern pattern of summer precipitation in China [23], the Changma in Korea, and the Baiu in Japan. In this study, we use 850 hPa geopotential heights to depict the interannual variability of the WNPSH and to define a WNPSH index (WNPSHI) as the JJA-mean 850 hPa height anomalies averaged over the region (110°–150°E, 10°–30°N), following Lu [17]. This index measures the year-to-year zonal displacement of the WNPSH. A positive (negative) WNPSHI indicates the westward extension (eastward retreat) of the subtropical high. The EAJ index (EAJI) is defined by using the difference between the 200 hPa zonal winds averaged over (120°–150°E, 30°–40°N) and (120°–150°E, 40°–50°N) to measure the meridional displacement of the EAJ, by following Lu [18]. A positive (negative) EAJI indicates a southward (northward) displacement of the EAJ.

2 Projected temporal evolution of EASR interannual variability

Figure 1 shows the evolution of the nine-year window running interannual variability of the EASRI under scenario A1B. The obvious feature is that the EASRI interannual variability experiences two prominent changes in the 21st century (Figure 1, MME). The intensity of interannual variability does not exhibit a clear change before the 2030s, with a fluctuation within the range of ±0.02 mm/d. The first prominent change occurs in the 2030s, with a small change before and a large persistent increase afterward. The intensity of the EASRI interannual variability is projected to be up to approximately 0.53 mm/d in the 2070s, representing an increase of approximately 30% relative to the early 21st century. Then, the second prominent change occurs, with a rapid decrease afterward. At the end of the 21st century, the intensity exhibits an increase of approximately 12% in ratio relative to the early 21st century, indicating that the occurrences of droughts and floods will experience phasic variation in the 21st century under scenario A1B. Especially in the 2070s, more frequent and serious flood disasters will happen due to the enhancement of both precipitation interannual variability and climatological mean precipitation [3, 5, 8].

In order to evaluate the MME result, the EASRI interannual variability in the individual models is calculated (Fig-

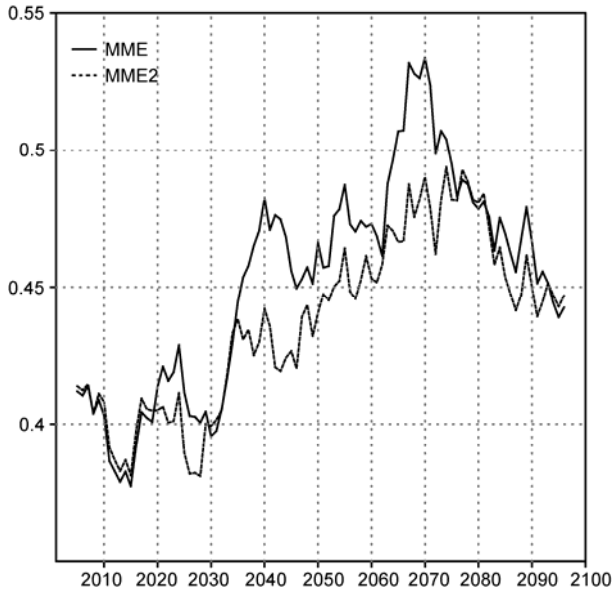

Figure 1 The MME (solid line, 18 models) and MME2 (dashed line, 17 models except hadcm3) results of the nine-year window running interannual variability of the EASRI under scenario A1B. Unit: mm/d.

ure 2). Almost all the models project prominent changes of East Asian summer rainfall interannual variability, with an increasing trend. Fifteen of the 18 selected models (except fgoals, gfdl2.1 and pcm) project prominent changes during the 2030s–2040s, with rapid increases afterward in the 21st century.

Among the 18 selected models, 17 project a spread of the EASRI interannual variability ranging from 0.2 to 0.7 mm/d, while it is up to 0.2–1.1 mm/d in the model hadcm3 (Figure 2), which is much higher than that of other models. Therefore, the 17-model MME is calculated except hadcm3 (Figure 1, MME2). It shows that the EASRI interannual variability also experiences two prominent changes in the 21st century, which is the same as the MME result. The two prominent changes also occur around the 2030s and 2070s, with an increase and decrease afterward, respectively. The model hadcm3 weakens the intensities of the MME2 EASRI interannual variability during the period of the 2030s–2070s, but it still increases by approximately 20% relative to the early 21st century.

The Mann-Kendall test method is used to ascertain the time when the abrupt changes occur in individual models and two MME results (Table not shown). The abrupt changes happen in the years 2034 and 2043 for the MME and MME2 results, with a tendency to increase afterward. Among the 15 models (except fgoals, gfdl2.1 and pcm), 11 project abrupt changes that occur in the period of the 2030s–2040s, with a tendency to increase afterward. The results indicate consistency among the projected changes of the EASRI interannual variability in individual models and the two MME results, although the Mann-Kendall test method does not detect the abrupt change around the 2070s.

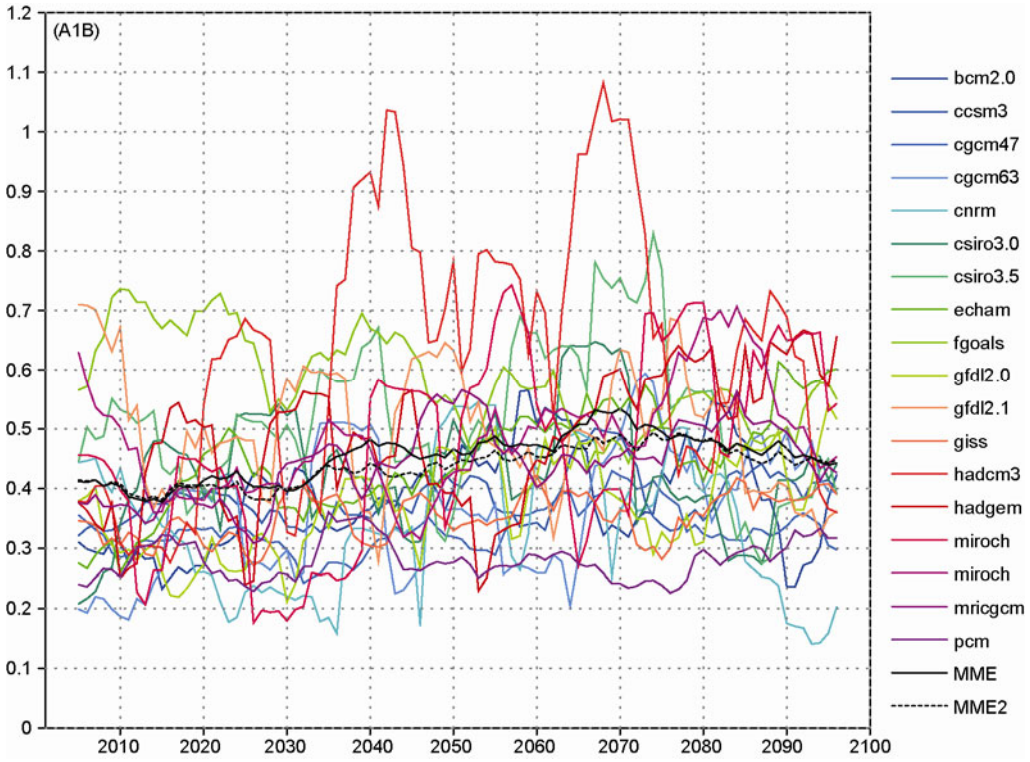

Figure 2 Same as in Figure 1, but for individual models. The black solid line represents the MME based on 18 models, and the black dashed line represents the MME2 based on 17 models. Unit: mm/d.

Otherwise, all the following results are the 18 models' MME projections unless specified otherwise, given that hadcm3 has no essential effect on the projected MME results.

Figure 3 shows the time-latitude cross-section of East Asian summer rainfall interannual variability averaged over 100°–160°E. The interannual variability of the summer rainfall is projected to exhibit prominent changes in the regions between 10°N and 50°N. The intensity is enhanced with time in two zonally oriented rain belts. The northern enhancement belt is at approximately 30°N, and its region is approximately the same as the climatological summer rain belt in East Asia and the western North Pacific, which is referred to as Meiyu in China, Changma in Korea, and Baiu in Japan. Generally, it is named the Meiyu rain belt in this study. Over the Meiyu rain belt, the precipitation interannual variability experiences an abrupt change around the 2030s and a consistent increase with a maximum in the 2070s. Then, the variability experiences another abrupt change and decreases later until the end of the 21st century. Besides this extratropical belt, the other belt-like region of enhanced projection variability is south of 20°N and is approximately the same as the climatological summer rain belt over the Philippine Sea and western North Pacific. The change of precipitation variability has a similar character with that of the Meiyu rain belt, which changes abruptly around the 2030s and 2070s, but is much stronger.

In a word, the interannual variability of East Asian summer rainfall is projected to experience two prominent changes in the 21st century under scenario A1B. The changes occur around the 2030s and 2070s, with consistent tendencies to increase and decrease afterward, respectively, with a maximum in the 2070s. This projection is consistent in the individual models and MME results, suggesting the result is reliable.

Furthermore, as for the spatial pattern change of precipitation interannual variability in different evolutions in the 21st century, we still have a paucity of knowledge. Therefore, three periods are selected, 2011–2030, 2041–2060, and 2071–2090, based on Figure 1 to analyze the spatial pattern change of precipitation variability.

Figure 4 shows the spatial pattern change in the interannual variability of East Asian summer rainfall in different periods of the 21st century. In the early period (Figure 4(a)), the change has a regional discrepancy in East Asia. Except for the negative change in southwestern China, a slightly positive change appears in the Meiyu rain belt, and a significant enhancement appears in northeast China. In the middle period (Figure 4(b)), the positive change appears in almost all of East Asia. The enhancement of variability tends to be predominant along the Meiyu rain belt and in the tropical western North Pacific. With the exception of the middle and lower reaches of the Yangtze (Changjiang) River, the enhancement of variability is significant at the 5% level over the Meiyu rain belt by the *F*-test. Compared with early 21st century (Figure 4(c)), the interannual variability increases by approximately 0.1–0.2 mm/d and is significant at the 5% level in southwestern China, Korea, and Japan, except for the middle and lower reaches of the Yangtze (Changjiang) River. In southeastern China, the interannual variability turns from significantly negative to significantly positive, exceeding 0.2 mm/d in amplitude, indicating that the occurrence of flood disasters will be more frequent. In the late

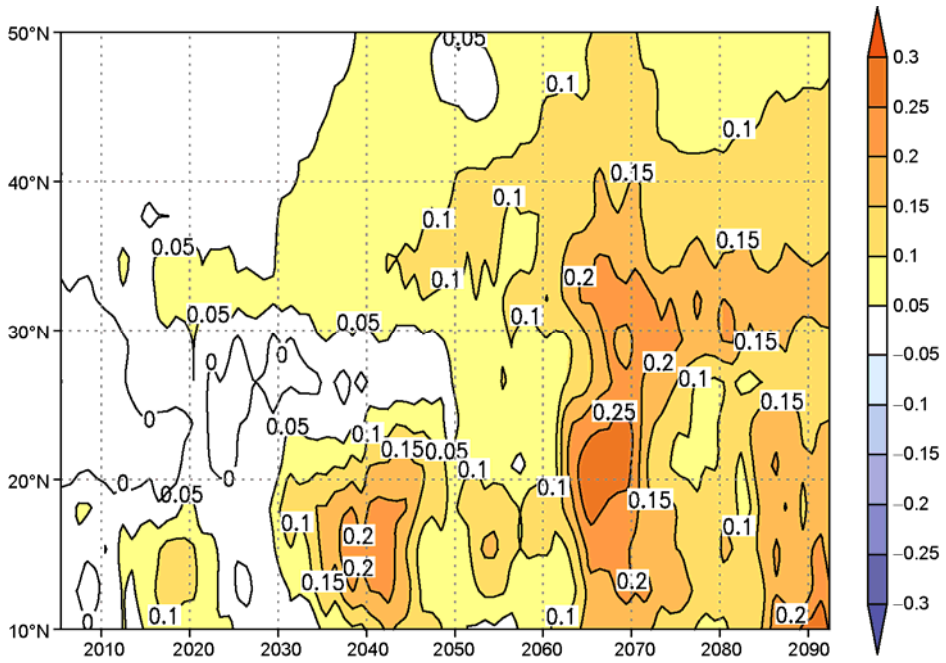

Figure 3 Time-latitude cross-section of changes in the interannual variability of East Asian summer rainfall averaged in 100°–160°E in the 21st century (relative to the 20th century). Unit: mm/d.

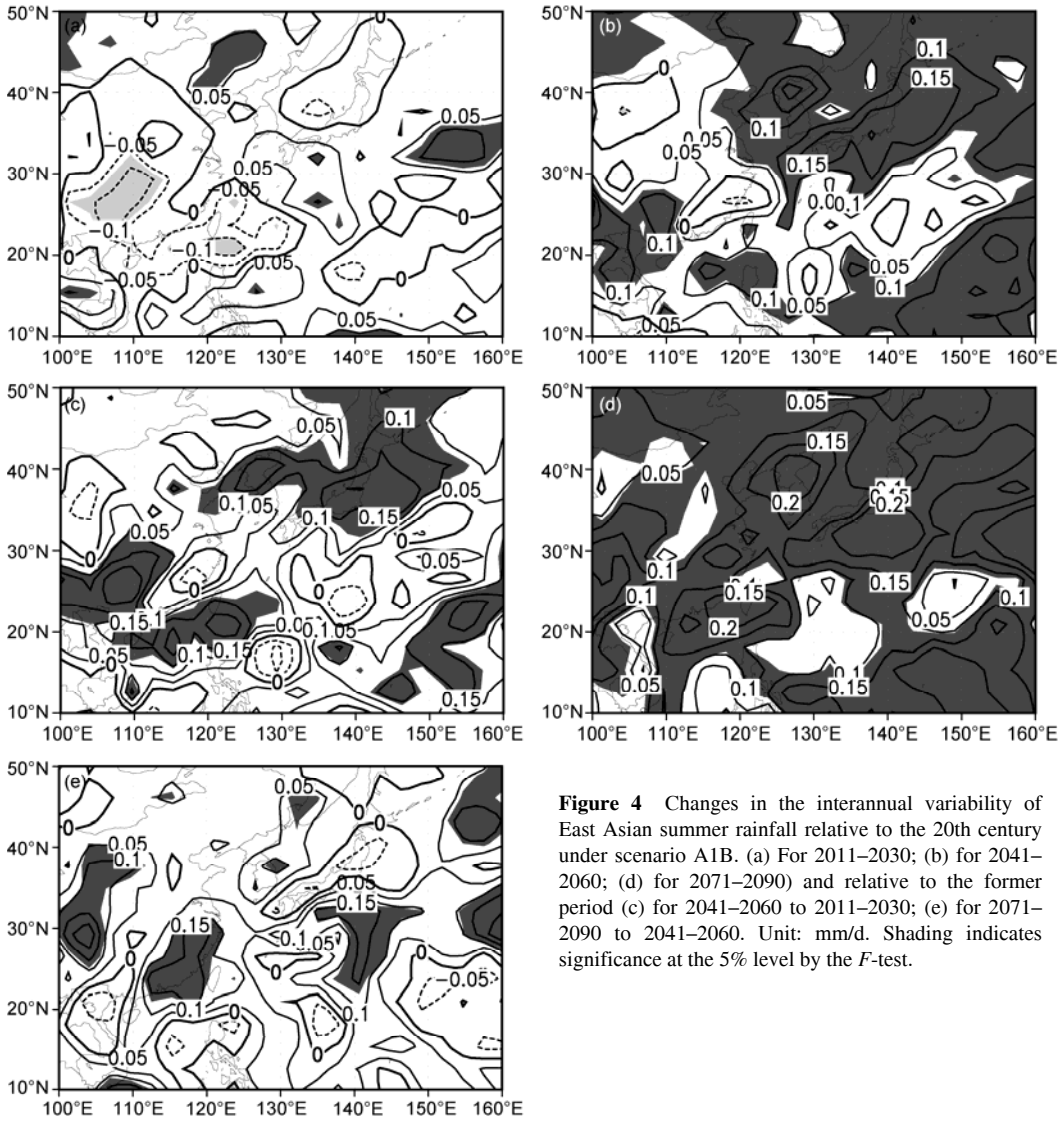

Figure 4 Changes in the interannual variability of East Asian summer rainfall relative to the 20th century under scenario A1B. (a) For 2011–2030; (b) for 2041–2060; (d) for 2071–2090) and relative to the former period (c) for 2041–2060 to 2011–2030; (e) for 2071–2090 to 2041–2060. Unit: mm/d. Shading indicates significance at the 5% level by the *F*-test.

period (Figure 4(d)), the enhanced interannual variability of East Asian summer rainfall prevails over the entire East Asia region. However, relative to middle period (Figure 4(e)), the variability is projected to be weakened in Japan, and no clear change in the middle and lower reaches of the Yangtze (Changjiang) River and the Korean Peninsula, suggesting a suppressed precipitation variability in late 21st century.

3 Projected changes in interannual variability of circulation

As noted before, the interannual variability of East Asian summer precipitation is found to be closely related to local circulation as well as that in the western North Pacific. A more (less) precipitation corresponds to a westward (eastward) displacement of the WNPSH [17]. An above (below)-normal precipitation corresponds to a southward (northward) displaced EAJ [18]. The relationships of climatological East Asian summer rainfall with the climatological WNPSH and EAJ remain robust in the 21st century [11]. Thus, are the relationships still maintained in the interannual variability?

For each model, the temporal evolution of the nine-year window running interannual variability of the WNPSHI and EAJI are calculated; then the correlations are calculated separately with the EASRI temporal variability, and finally, the MME correlation coefficient is computed, following Annamalai et al. [24]. The correlation coefficients of the EASRI interannual variability with the WNPSHI and EAJI variability are 0.21 and 0.37 under scenario A1B, respectively, and are statistically significant at the 5% level. This result suggests that an enhanced (suppressed) WNPSH interannual variability corresponds to a stronger (weaker) WNPSH zonal displacement variability and leads to an in-

tensified (weakened) East Asian summer rainfall interannual variability. An intensified (weakened) EAJ variability corresponds to a stronger (weaker) EAJ meridional displacement variability and leads to an increased (decreased) precipitation variability.

Therefore, the projected changes in interannual variability of the WNPSH, EAJ, water vapor transport, and precipitable water are investigated to prove the projected change of precipitation interannual variability, given that the simulations are likely more reliable for large-scale circulation than for precipitation.

3.1 Projected temporal evolution of WNPSH interannual variability

Figure 5(a) displays the time-latitude cross-section of geopotential height interannual variability changes at 850 hPa averaged over 110°–150°E relative to the 20th century under scenario A1B. The interannual variability experiences an obvious phasic variation in East Asia, especially in the regions between 10°N and 30°N. The variability evolves a fluctuation of "–""+""–" at an amplitude of ±0.4 hPa before the 2030s and a substantial increase after the 2030s, with a maximum of 1.0 hPa in the 2070s, when the turning point appears. By the end of the 21st century, the variability decreases to -0.8hPa relative to the 20th century. The results suggest that the WNPSH interannual variability exhibits a slight fluctuation in the early 21st century and a consistent increase during the period of the 2030s–2070s, then a rapid decrease in late 21st century, which is the same as the temporal evolution of the summer precipitation interannual variability. An enhanced WNPSH interannual variability corresponds to an enhanced precipitation interannual variability, and vice versa.

Figure 6 shows the spatial pattern of the WNPSH interannual variability changes at 850 hPa in 2011–2030, 2041–2060, and 2071–2090 relative to the 20th century. In 2011–2030 (Figure 6(a)), the interannual variability of the 850 hPa geopotential height is slightly decreased in East Asia and the western North Pacific. In 2041–2060 (Figure 6(b) and (c)), the geopotential height interannual variability is significantly enhanced in East Asia and the western North Pacific, with a maximum of 0.6 hPa and significantly suppressed maximum of 0.8 hPa over the northern edge of the WNPSH (30°–40°N), which demonstrates greater zonal displacement variability and a smaller meridional displacement variability. In 2071–2090 (Figure 6(d)), the spatial patterns of interannual variability changes are contrary to those in 2041–2060. The interannual variability of the 850 hPa geopotential height is significantly weakened in the region south of 30°N and significantly enhanced in the region north of 30°N, with amplitudes of 0.6 hPa, which are statistically significant at the 5% level by the F-test. In the late 21st century, the interannual variability of the WNPSH is much weaker than that in the 20th century and is much weaker than that in the early and middle 21st century (Figure 6(e)). These results clearly demonstrate that a prominent change occurs around the 2070s, with a rapid decrease afterward.

3.2 Projected temporal evolution of EAJ interannual variability

The changes of zonal wind interannual standard deviations at 200 hPa also experience physical variation in the 21st century (Figure 5(b)). The intensified variability mainly appears over two zonally-oriented belts of 30°–40°N and 40°–50°N, which are approximately the same as those showing climatological strong zonal wind variability in observation [11] and clearly overlap the two averaging areas used for the definition of the EAJI. The suppressed variability mainly changes along roughly 40°N, where the axis of the EAJ is located. In the northern side of the EAJ (40°–50°N), the interannual zonal wind variability exhibits two prominent changes around the 2030s and 2070s. The variability is projected to continually increase during the 2030s–2070s, and decrease before the 2030s and after the 2070s. In the southern side of the EAJ (30°–40°N), the interannual variability increases before the 2030s and decreases until the end of the 21st century except for a short increase around the 2060s. The results suggest that the EAJ interannual variability experiences a physical variation in the 21st century. The nine-year window running interannual variability of the EAJI (Figure not shown) also evolves clearly in the same way. The temporal evolution of the EAJ is quite similar to that of the East Asian summer rainfall, which suggests that an enhanced (suppressed) EAJ interannual variability leads to an intensified (weakened) interannual variability of precipitation.

The spatial patterns of the interannual standard deviation of the zonal wind at 200 hPa in the 21st century also clearly demonstrate the changes (Figure 7). In the early 21st century (Figure 7(a)), the zonal wind interannual variability is projected to be significantly decreased roughly along the axis of the EAJ, with no appreciable changes in the northern and southern side of the EAJ, suggesting that the interannual variability of the meridional displacement of the EAJ is nearly unchanged and the intensity is decreased during this period. In the middle 21st century (Figures 7(b) and (c)), the zonal wind variability is significantly enhanced in the northern side of the EAJ relative to the 20th century and early 21st century and is slightly suppressed in the southern side, suggesting the displacement variability is significantly enhanced. In the late 21st century (Figure 7(d)), the variability is slightly increased in the northern side and decreased in the southern side of the EAJ, indicating a slight increase of the EAJ interannual variability relative to the 20th century. Compared with the middle 21st century (Figure 7(e)), the variability is deceased on both sides of the EAJ, which

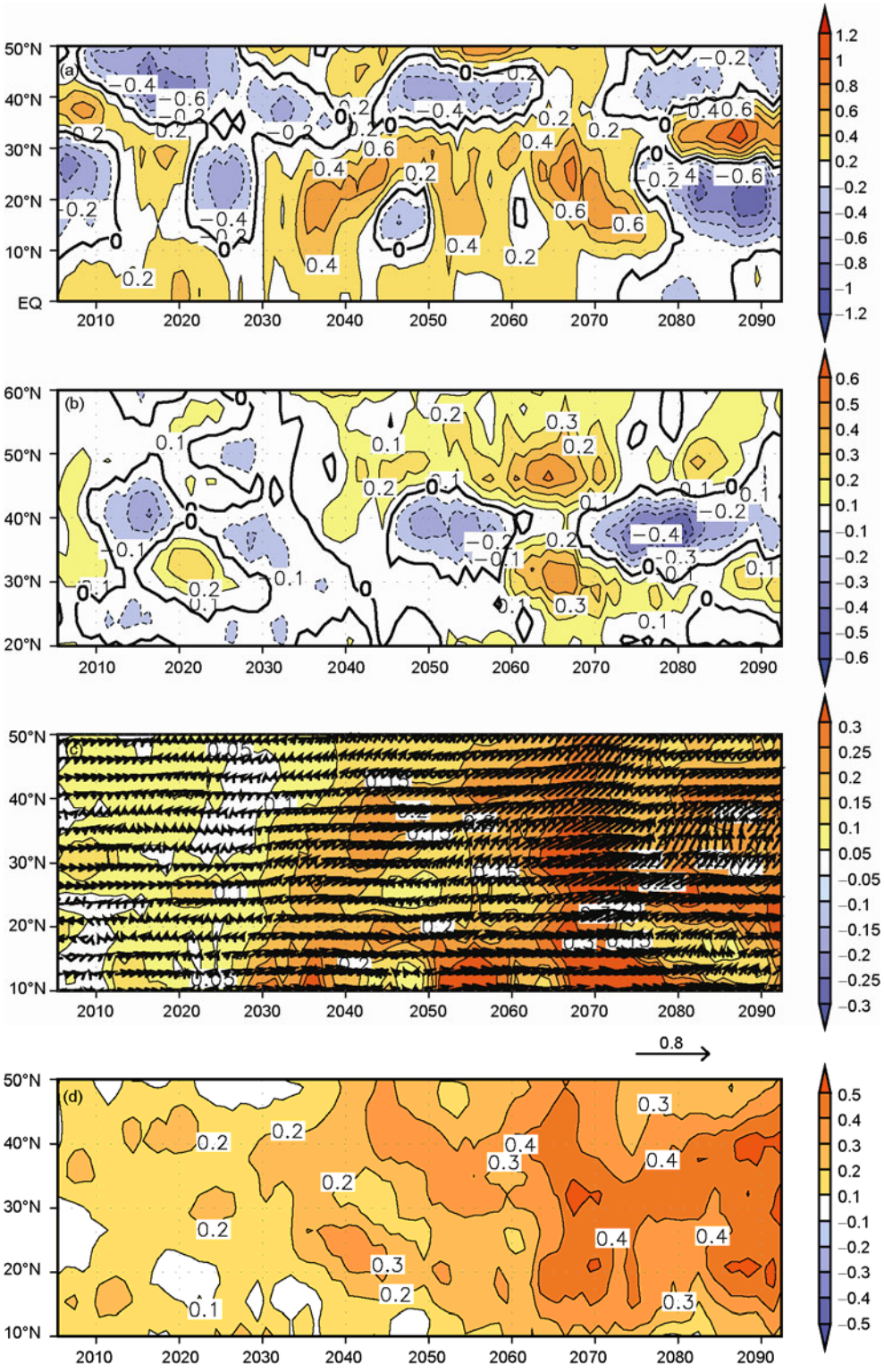

Figure 5 Same as in Figure 3, but for geopotential height at 850 hPa averaged in 110°–150°E ((a) in hPa), zonal wind at 200 hPa averaged in 120°–150°E ((b) in m/s), water vapor transport at 850 hPa averaged in 110°–160°E ((c) in g/(s hPa cm)) and precipitable water averaged in 100°–160°E ((d) in kg/m^2) (relative to the 20th century).

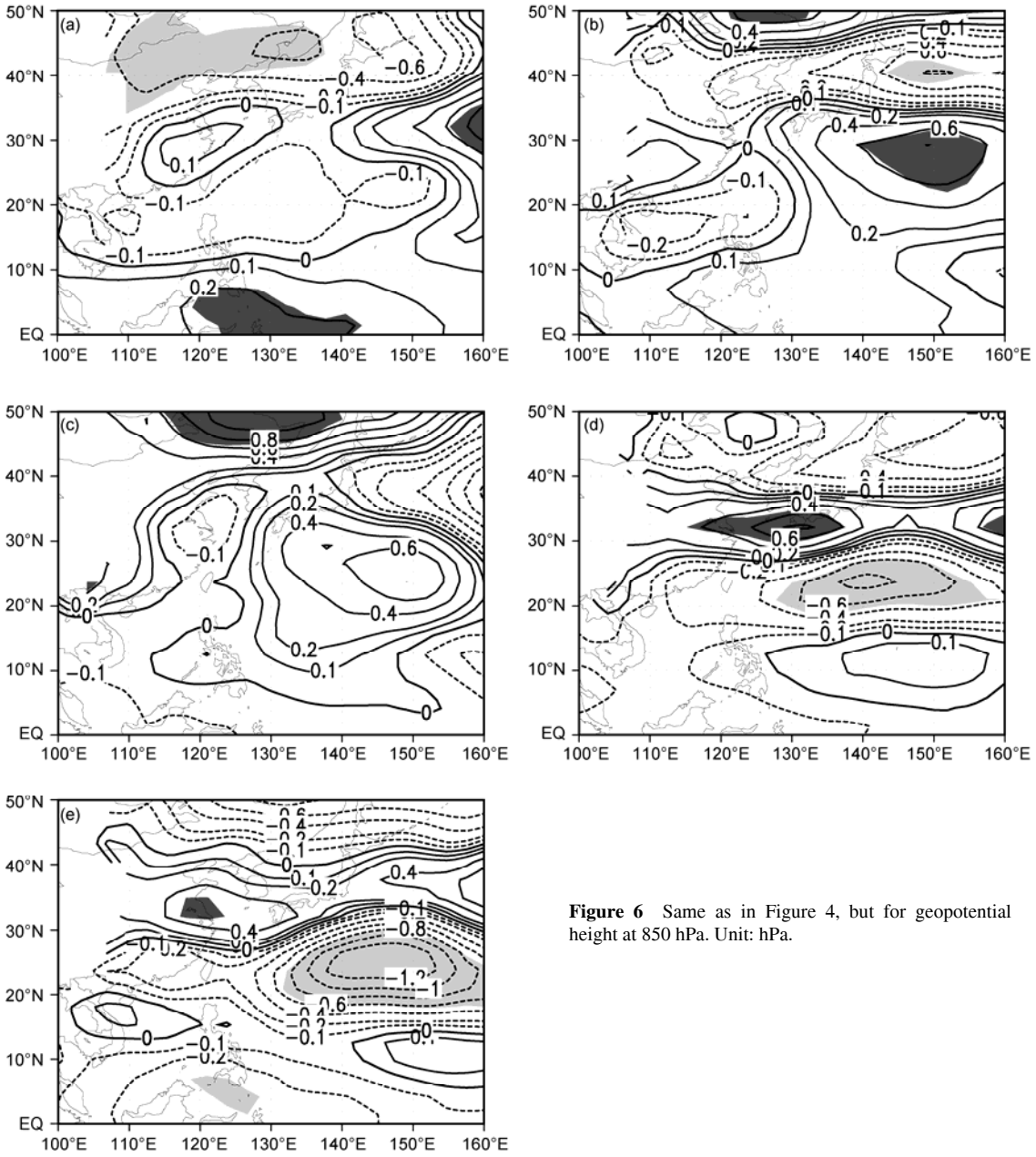

Figure 6 Same as in Figure 4, but for geopotential height at 850 hPa. Unit: hPa.

suggests that the EAJ interannual variability is weaker than that in the middle period. Therefore, the study suggests that the interannual variability of the EAJ is expected to exhibit a phasic variation in the 21st century.

3.3 Projected temporal evolution of water vapor transport interannual variability

The 17-model (except hadcm3, for lack of data) MME (Figure 5(c)) shows that the changes in the interannual variability of the East Asian summer water vapor transport experiences an obvious phasic variation, and the enhanced variability appears to have two zonally oriented belts in the regions between 10°N and 50°N. Over the northern belt, which is the Meiyu rain belt, the interannual variability of water vapor transport increases slightly before the 2030s. The westerly transport variability appears in the region of approximately 30°N, and the northward transport variability turns from southwesterly to southeasterly in the region between 30°N and 40°N before the 2030s. From the 2030s to 2070s, the southwesterly water vapor transport variability displays a continuous intensification in the regions between 10°N and 50°N, reaching a maximal transport of more than 0.3 g/(s hPa cm) by the 2070s. Then, the northeastward transport variability decreases after the 2070s, with an intensification of 0.2 g/(s hPa cm) by the end of the 21st century. Over the southern belt, southward of 20°N, the water vapor transport interannual variability also experiences two prominent changes around the 2030s and 2070s, with the same physical variations of those over the northern belt. The

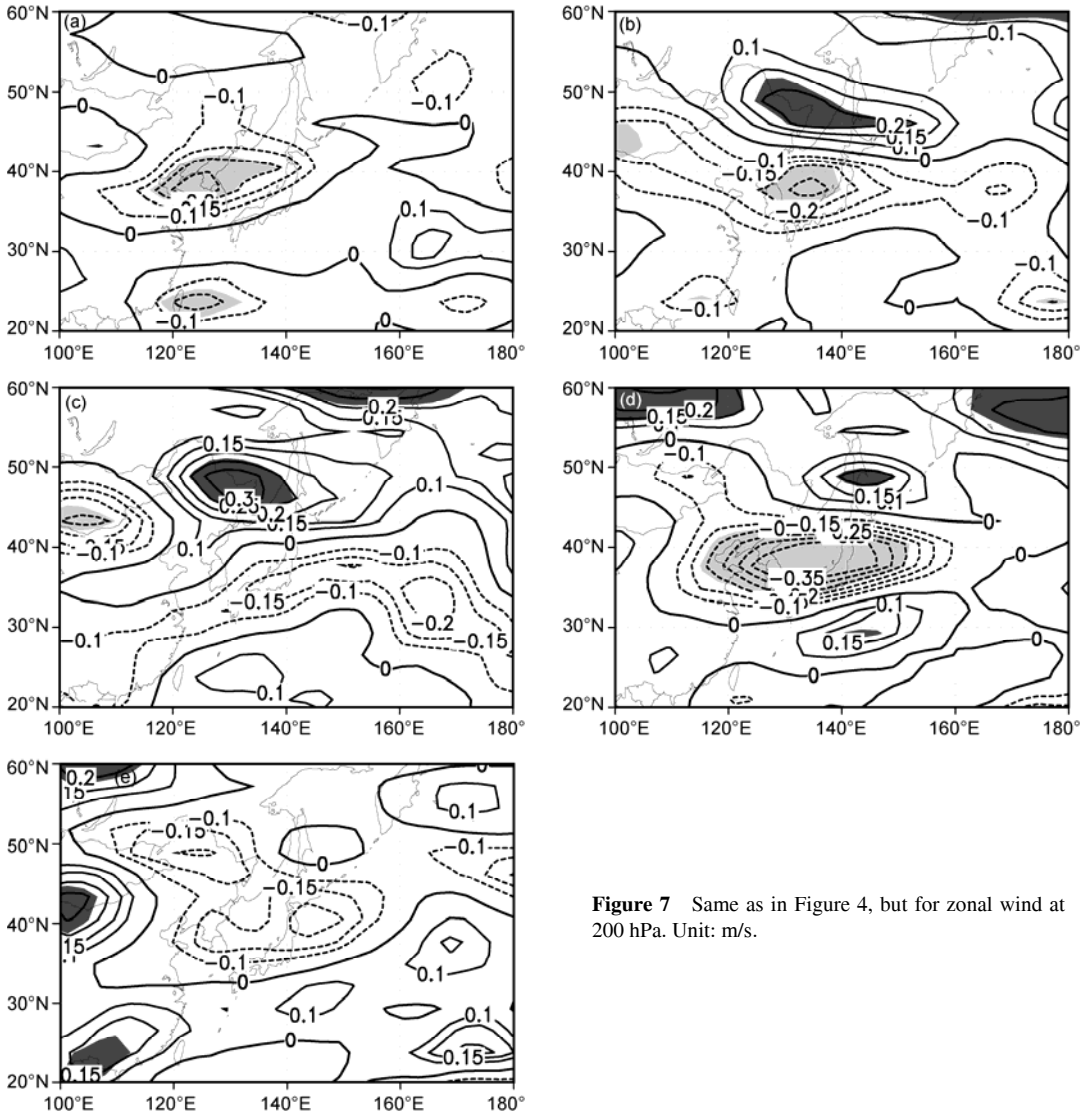

Figure 7 Same as in Figure 4, but for zonal wind at 200 hPa. Unit: m/s.

temporal evolution is consistent with that of the precipitation interannual variability in East Asia, suggesting that the changes of water vapor transport interannual variability is also a key factor resulting in the changes of precipitation variability.

Figure 8 further shows the changes in the spatial pattern of the water vapor transport interannual variability over East Asia and the western North Pacific. In the early 21st century (Figure 8(a)), the transport interannual variability appears to have an inconsistent change over this region. The insignificant westerly water vapor transport variability appears in the middle and lower reaches of the Yangtze (Changjiang) River, and an insignificant easterly transport variability appears in south Japan. In the middle 21st century (Figure 8(b)), the intensified transport variability east of 115°E is statistically significant at the 5% level by the *F*-test. A northeastward water vapor transport interannual variability forms from the Arab Sea through the Indian Ocean and all the way to the South China Sea. The water vapor variability transported into eastern China mainly comes from its western side and the water vapor into the Korean Peninsula and Japan from its southern and eastern side. The water vapor transported to the Meiyu rain belt is significantly intensified relative to early period (Figure 8(c)), with a maximum of 0.3 g/(s hPa cm) in north Japan. In the late 21st century (Figure 8(d)), the interannual variability of the northeastward water vapor transport is enhanced. However, the easterly transport variability appears in south Japan and the East China Sea (Figure 8(e)) because of the appearance of an anomalous cyclone located over the western North Pacific, leading to a suppressed interannual variability relative to the middle 21st century.

3.4 Projected temporal evolution of precipitable water interannual variability

In the East Asian summer monsoon region, the interannual variability of precipitable water is persistently intensified in

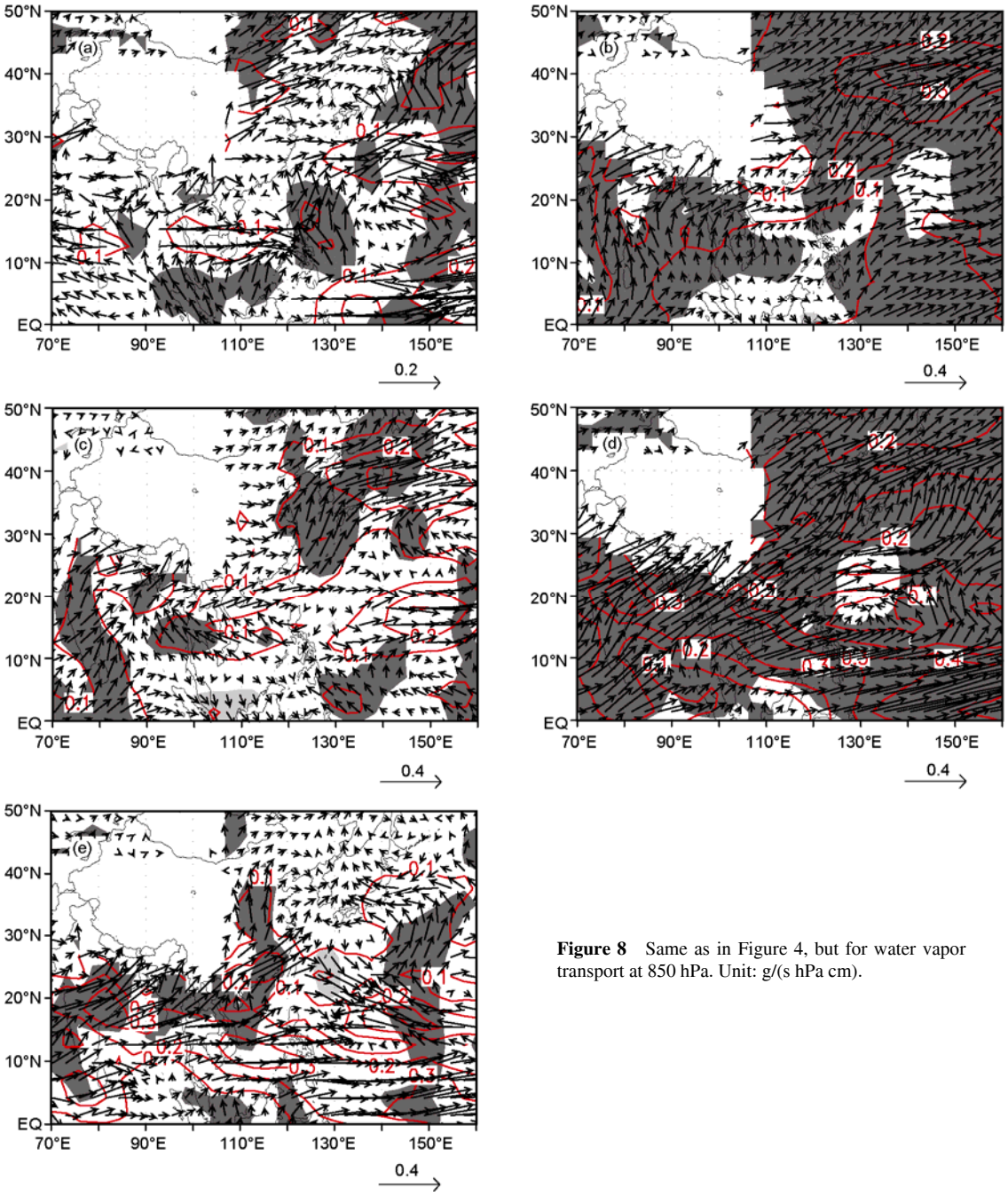

Figure 8 Same as in Figure 4, but for water vapor transport at 850 hPa. Unit: g/(s hPa cm).

the 21st century under scenario A1B (Figure 5(d)), from 0.1 kg/m^2 in the early part to 0.5 kg/m^2 by the end of the century. The variability experiences two abrupt increases around the 2030s and 2060s. The intensification of precipitable water interannual variability implies an enhancement of precipitation source variability and the enhancement of precipitation interannual variability.

The spatial pattern of the changes in the precipitable water interannual variability further demonstrates the liner increases (Figure 9) in the 21st century. In the early period (Figure 9(a)), the intensification of variability appears in most regions of East Asia and the western North Pacific except in eastern China and the South China Sea. In the middle period (Figure 9(b)), the intensification covers all of East Asia and the western North Pacific, with a maximum of 0.4 kg/m^2. Compared with the early period, the strongest enhancement appears over the Meiyu rain belt, with a maximum of 0.3 kg/m^2 (Figure 9(c)), indicating a great intensification in potential precipitation interannual variability. By the late period (Figure 9(d)), the spatial pattern of variability changes is basically consistent with that in the middle of the 21st century, but the intensity is continuously increased. Especially in the region from central East China northeastward into the North Pacific through Korea and Japan, the interannual variability increases up to 0.5 kg/m^2. Compared with the middle period, there is only a slight

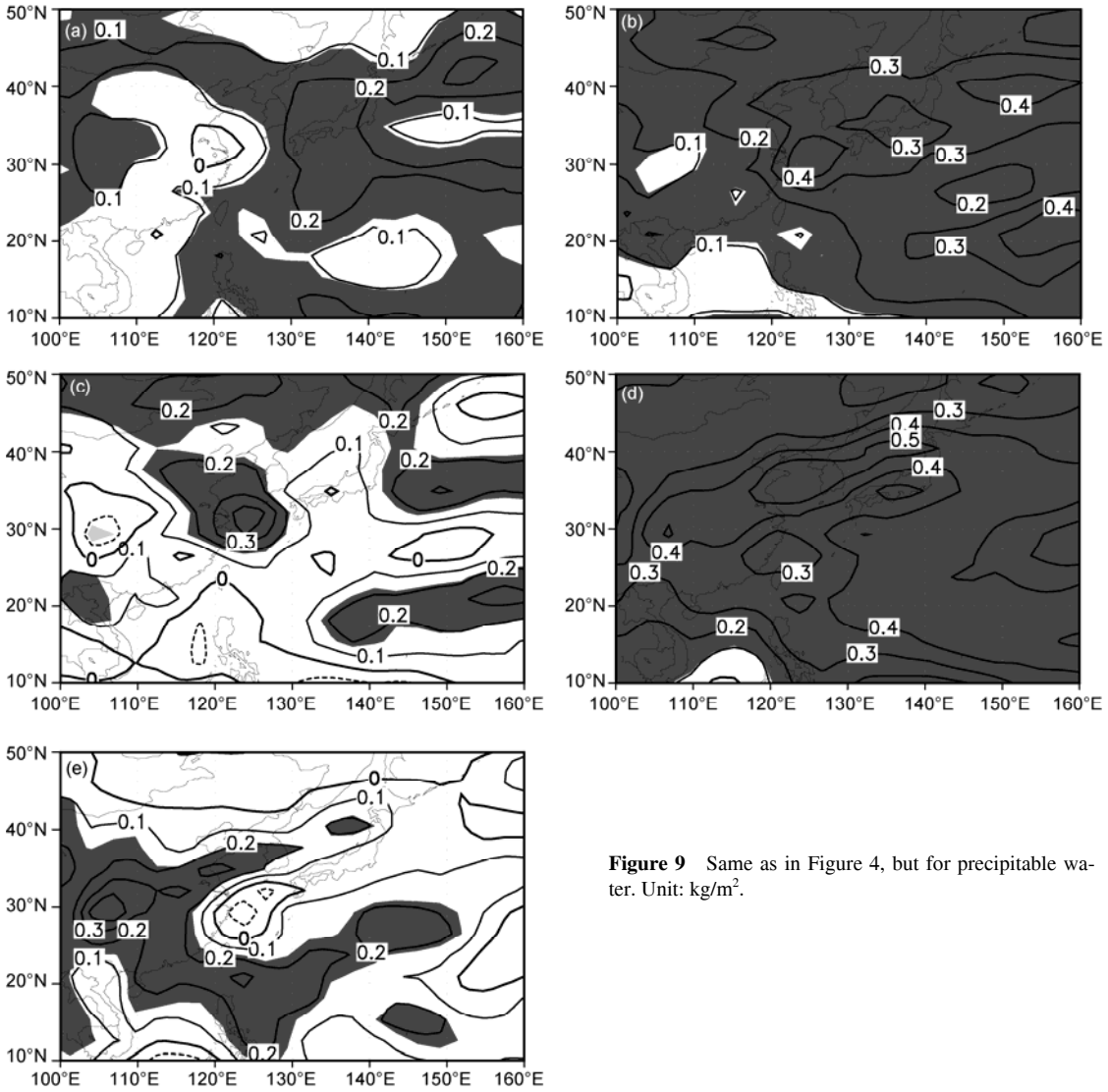

Figure 9 Same as in Figure 4, but for precipitable water. Unit: kg/m^2.

decrease over the East China Sea (Figure 9(e)).

4 Discussion and conclusions

In this study, the projected temporal evolution in interannual variability of the East Asian summer rainfall in the 21st century is investigated by analyzing the simulated results of 18 CMIP3 models under the A1B scenario. The precipitation interannual variability is projected to experience two prominent changes in the 21st century. The first prominent change occurs around the 2030s, with a small change before and a large increase afterward. The precipitation variability is projected to be up to approximately 0.53 mm/d in the 2070s, representing an increase of approximately 30% relative to the early 21st century. The second change happens around the 2070s, with a decrease afterward. By the end of the 21st century, the increase is approximately 12% relative to the early period. This result suggests that droughts and floods will occur much more frequently after the 2030s. Especially around the 2070s, more frequent and serious flood disasters will happen because of the enhancement of both of the precipitation variability and climatological mean precipitation [3, 5, 8].

The MME result also projects two prominent changes in the interannual variability of the WNPSH and EAJ. The change in interannual variability of the WNPSH is characterized by zonal displacement and that of the EAJ by meridional displacement. The WNPSH and EAJ variability experience slight fluctuations in the early 21st century and persistently increase during the 2030s and 2070s, and then decrease rapidly after the 2070s. By the end of the 21st century, the interannual variability of the WNPSH is suppressed and that of the EAJ is enhanced relative to the 20th century. The temporal evolutions of the WNPSH and EAJ are consistent with that of the East Asian summer rainfall.

The interannual variability of water vapor transport at 850 hPa is also projected to experience two prominent

changes. Over the Meiyu rain belt, the transport variability changes slightly before the 2030s and substantially increases afterward until the 2070s, with a maximum of 0.3 g/(s·hPa·cm) relative to the 20th century. The variability turns to decrease after the 2070s, and with an enhancement of 0.2 g/(s·hPa·cm) by the end of the 21st century relative to the 20th century. The change process in the interannual variability of water vapor transport agrees well with that of the precipitation.

Furthermore, the interannual variability of precipitable water is projected to intensify all over East Asia and the western North Pacific, with an increase from 0.1 kg/m^2 in the early part to 0.5 kg/m^2 by the end of the 21st century. The variability experiences two abrupt increases around the 2030s and 2060s. The intensification of precipitable water interannual variability implies an enhancement of precipitation source variability and an enhancement in the interannual variability of East Asian summer rainfall.

The phasic variation of interannual variability of East Asian summer rainfall is caused by variability of both the dynamic and thermodynamic variables under the A1B scenario. In the early and middle 21st century, both factors favor the intensification of precipitation interannual variability. In late 21st century, the dynamic factors suppress the precipitation variability while the thermodynamic factor intensifies the precipitation variability.

However, great uncertainties still exist in numerical climate projections for future climate [14, 15]. The uncertainties mainly come from the climate model uncertainty, future scenario uncertainty, and internal variability uncertainty. The simulations will be much more determinate with the development of climate models, the improvement of scenarios, and the understanding of climate systems and related feedbacks. The simulated results of CMIP5 models provide a good basis for better understanding the uncertainty in the present study. The investigation supplies a reference for further analyzing the projected change in the interannual variability of East Asian precipitation by using the CMIP5 experiment results.

We thank three anonymous reviewers for their comments and suggestions. We acknowledge the modeling groups, which produced the simulations, and the Program for Climate Model Diagnosis and Inter-comparison (PCMDI) and the WCRP's Working Group on Coupled Modeling (WGCM) for their roles in making the WCRP CMIP3 multi-model dataset available. Support of this dataset is provided by the Office of Science, U.S. Department of Energy. This work was supported by Special Scientific Research Fund of Meteorological Public Welfare Profession (Grant No. GYHY200906020) and National Basci Research Program of China (Grant No. 2010CB950304).

1 Kripalani R H, Oh J H, Chaudhari H S. Response of the East Asian summer monsoon to doubled atmospheric CO_2: Coupled climate model simulations and projections under IPCC AR4. Theor Appl Climatol, 2007, 87: 1–28
2 Wang H J, Zeng Q C, Zhang X H. The numerical simulation of the climatic change by CO_2 doubling. Sci China Ser B-Chem, 1993, 36: 451–462
3 Buehc. Simulation of the future change of East Asian monsoon climate using the IPCC A2 and B2 scenarios. Chin Sci Bull, 2003, 48: 1024–1030
4 Min S K, Park E H, Kwon W T. Future projections of East Asian climate change from multi-AOGCM ensembles of IPCC SRES scenario simulations. J Meteorol Soc Jpn, 2004, 82: 1187–1211
5 Ashirt R G, Kitoh A, Yukimoto S. Transient response of ENSO–monsoon teleconnection in MRI_CGCM2.2 climate change simulations. J Meteorol Soc Jpn, 2005, 83: 273–291
6 Kitoh A, Hosaka M, Adachi Y, et al. Future projections of precipitation characteristics in East Asia simulated by the MRI CGCM2. Adv Atmos Sci, 2005, 22: 467–478
7 Xu Y L, Zhang Y, Lin Y H, et al. Analyses on the climate change responses over China under SRES B2 scenario using PRECIS. Chin Sci Bull, 2006, 51: 2260–2267
8 Sun Y, Ding Y H. A projection of future changes in summer precipitation and monsoon in East Asia. Sci China Earth Sci, 2010, 53: 284–300
9 Li H M, Feng L, Zhou T J. Multi-model projection of July–August climate extreme changes over China under CO_2 doubling. Part I: Precipitation. Adv Atmos Sci, 2011, 28: 433–447
10 Feng L, Zhou T J, Wu B, et al. Projection of future precipitation change over China with a high-resolution global atmospheric model. Adv Atmos Sci, 2011, 28: 464–476
11 Lu R Y, Fu Y H. Intensification of East Asian summer rainfall interannual variability in the twenty-first century simulated by 12 CMIP3 coupled models. J Clim, 2010, 23: 3316–3331
12 Kang I S, Jin K, Wang B, et al. Intercomparison of the climatological variations of Asian summer monsoon precipitation simulated by 10 GCMs. Clim Dyn, 2002, 19: 383–395
13 Jiang D B, Wang H J, Lang X M. Evaluation of East Asian climatology as simulated by seven coupled models. Adv Atmos Sci, 2005, 22: 479–495
14 Li B, Zhou T J. Projected climate change over China under SRES A1B scenario: Multi-model ensemble and uncertainties (in Chinese). Adv Clim Change Res, 2010, 6: 270–276
15 Jiang D B, Fu Y H. Climate change over China with a 2°C global warming (in Chinese). Chin J Atmos Sci, 2012, 36: 234–246
16 Lu R Y, Lin Z D. Role of subtropical precipitation anomalies in maintaining summertime meridional teleconnections over the western North Pacific and East Asia. J Clim, 2009, 22: 2058–2072
17 Lu R Y. Indices of the summertime western North Pacific subtropical high. Adv Atmos Sci, 2002, 19: 1004–1028
18 Lu R Y. Associations among the components of the East Asian summer monsoon system in the meridional direction. J Meteorol Soc Jpn, 2004, 82: 155–165
19 Meehl G A, Stocker T F, Collins W D, et al. Global Climate Projections. In: Climate Change 2007: The Physical Science Basis. Contribution of Working Group I to the Fourth Assessment Report of the Intergovernmental Panel on Climate Change. In: Solomon S, Qin D, Manning M, et al, eds. Cambridge, United Kingdom and New York: Cambridge University Press, 2007. 748–845
20 Zhou T J, Yu R C. Twentieth-century surface air temperature over China and the global simulated by coupled climate models. J Clim, 2006, 19: 5843–5858
21 Xu C H, Shen X Y, Xu Y. An analysis of climate change in East Asia by using the IPCC AR4 simulations (in Chinese). Adv Clim Change Res, 2007, 3: 287–291
22 Jiang D B, Zhang Y, Sun J Q. Ensemble projection of 1–3°C warming in China. Chin Sci Bull, 2009, 54: 3326–3334
23 Zhou T J, Yu R C. Atmospheric water vapor transport associated with typical anomalous summer rainfall patterns in China. J Geophys Res, 2005, 110: D08104
24 Annamalai H, Hamilton K, Sperber K R. The South Asian summer monsoon and its relationship with ENSO in the IPCC AR4 simulations. J Clim, 2007, 20: 1071–109